Experimental and Modeling Study of $C_5H_{10}O_2$ Ethyl and Methyl Esters†

W. K. Metcalfe, S. Dooley, H. J. Curran,* J. M. Simmie, A. M. El-Nahas, and M. V. Navarro

Combustion Research Centre, National University of Ireland, Galway, Ireland

Received: November 15, 2006; In Final Form: December 20, 2006

Due to the world's over-reliance on fossil fuels there has been a developing interest in the production of renewable biofuels such as methyl and ethyl esters derived from vegetable oils and animal fats. To increase our understanding of the combustion chemistry of esters, the oxidation of methyl butanoate and ethyl propanoate, both with a molecular formula of $C_5H_{10}O_2$, have been studied in a series of high-temperature shock tube experiments. Ignition delay times for a series of mixtures, of varying fuel/oxygen equivalence ratios ($\phi = 0.25-1.5$), were measured behind reflected shock waves over the temperature range 1100−1670 K, and at pressures of 1.0, and 4.0 atm. It was found that ethyl propanoate was consistently faster to ignite than methyl butanoate, particularly at lower temperatures. Detailed chemical kinetic mechanisms have been assembled and used to simulate these experiments with good agreement observed. Rate of production analyses using the detailed mechanisms shows that the faster reactivity of ethyl propanoate can be explained by a six-centered unimolecular decomposition reaction with a relatively low activation energy barrier producing propanoic acid and ethylene. The elimination reaction itself is not responsible for the increased reactivity; it is the faster reactivity of the two products, propanoic acid and ethylene that leads to this behavior.

1. Introduction

In 2001 the transport sector contributed 21% of total greenhouse gas (GHG) emissions in the EU and was responsible for 32% of GHG emissions in the United States in 2002. Reducing GHG emissions throughout the world will require implementation of a variety of strategies, including the use of synthetic fuels to supplement petroleum-based gasolines. A particularly attractive class of synthetic fuels is oxygenated hydrocarbon liquid fuels; these fuels can readily be used in advanced diesel engines and diesel-hybrids because of the inherently high thermal efficiencies of these engines compared to spark ignition engines. These biodiesel fuels are also attractive because of their low sulfur content, which allows the use of a catalyst to remove NO_x from lean-burn engine exhaust (the catalyst does not get destroyed by sulfur) to meet new stringent, governmental emission standards. Biodiesel fuels are also renewable fuels, which have a low impact on global warming, and which can help limit dependence on foreign-derived fuel supplies. With oxygen content typically 10% or greater by mass,[1] biodiesel fuels may also provide soot-reduction benefits similar to those observed for other oxygenated diesel fuels and additives.[2]

Typical biodiesel fuels consist of mixtures of saturated and unsaturated methyl esters containing carbon chains 12 or more atoms in length.[1] Although methyl butanoate and ethyl propanoate do not have the high molecular weight of a biodiesel fuel, they do have the essential chemical structural features, namely the $RC(=O)OCH_3$ or $RC(=O)OC_2H_5$ structure (where R is an alkyl or alkenyl radical) and thus the resultant reaction mechanism is smaller and will be of more manageable size than that for a larger hydrocarbon.[3]

Numerous engine combustion studies have been performed using these methyl- and ethyl-ester fuels and their constituents.[4] There have been a number of studies suitable for comparison with chemical kinetic models in the pyrolysis regime. These studies were performed in a static reactor by Parsons et al.[5−7] in 1956 and by Hoare et al.[8] in 1967 but the results were more qualitative rather than quantitative in nature. Parsons et al. recorded the maximum value of the derivative of pressure with respect to time and defined this as the ignition delay time. In the experiments the pressure was recorded with a manometer and consequently the data would not have allowed resolution of pressure changes more quickly than every several seconds. Thus, the experimental results cannot be relied on for quantitative comparisons of reactivity profiles.

TABLE 1: Percentage Composition of Fuel/O_2/Ar Mixtures

ϕ	fuel	O_2	Ar
0.25	1.0	26.00	73.00
0.50	1.0	13.00	86.00
1.00	1.0	6.50	92.50
1.50	1.5	6.50	92.00

The only known detailed chemical kinetic models[9,10] have been used to simulate the data outlined above, but there is a need to generate more reliable data to understand the oxidation process and produce a detailed chemical kinetic mechanism that can accurately simulate the oxidation process under diesel engine conditions.

To this end, Marchese et al.[11] have studied the oxidation of methyl butanoate in a high-pressure flow reactor at a pressure of 12.5 atm, in the temperature range 500−900 K, using 800 ppm fuel at equivalence ratios of 0.35−1.5. Reactant, intermediate, and product species profiles were recorded as a function of reactor temperature for the mixtures at different equivalence ratios, together with simulated profiles calculated using the mechanism developed by Fisher et al.[10] Overall, the mechanism agreed well with experiments under stoichiometric conditions but underpredicted the observed reactivity under fuel-lean conditions and overpredicted the observed reactivity under fuel-rich conditions. Neither the model nor the experiments exhibited

† Part of the special issue "James A. Miller Festschrift".

* Corresponding author. E-mail: henry.curran@nuigalway.ie.

10.1021/jp067582c CCC: $37.00
Published on Web 02/07/2007

TABLE 2: Thermodynamic Properties for Selected Species

species	$\Delta_f H°(298\ K)$ (kcal mol^{-1})	$S°(298\ K)$ (cal mol^{-1} K^{-1})	C_p (cal mol^{-1} K^{-1})					
			300 K	400 K	500 K	600 K	800 K	1000 K
EP	−111.0	94.19	33.58	41.24	47.80	53.37	62.44	69.23
EP3J	−61.8	97.85	34.27	41.39	47.33	52.27	60.25	66.18
EP2J	−69.5	94.07	33.28	40.85	47.12	52.34	60.75	66.91
EPEJ	−65.5	96.04	34.21	41.76	48.01	53.09	61.01	66.67
EE	−105.7	84.59	27.38	33.54	39.10	43.87	51.34	57.03
EE2J	−59.2	84.55	28.26	34.31	39.46	43.74	50.29	55.16

a pronounced negative temperature coefficient (NTC) region (at a residence time of 1.8 s), but the production of formaldehyde provided evidence of low-temperature chemistry in both the model and experiments. The effect of low-temperature chemistry was most pronounced under fuel-lean conditions.

Data from the study of Marchese et al.[11] were also included in a more comprehensive study of methyl butanoate oxidation by Gail et al.[12] This study also presented new experimental results obtained in a jet stirred reactor at 0.101 MPa, $\phi = 1.13$, and the temperature range $800 \leq T \leq 1350$ K. In addition, new experimental data generated in an opposed-flow diffusion flame at 0.101 MPa were presented. These data were simulated using the mechanism developed by Fisher et al.,[10] with some modifications made to improve the overall agreement of the model.

Recently, Schwartz et al.[13] studied the effect of doping a methane/air premixed flame with 5000 ppm of methyl butanoate (MB) and ethyl propanoate (EP). In the case of EP they find that a unimolecular six-centered dissociation reaction explains their results:

$$C_2H_5COOC_2H_5 \rightarrow C_2H_5COOH + C_2H_4$$

whereas MB has a decomposition rate that is consistent with a unimolecular simple fission reaction:

$$C_3H_7COOCH_3 \rightarrow C_3H_7C(O)\dot{O} + \dot{C}H_3$$

The aim of *this study* is to provide more information on the combustion characteristics of methyl butanoate and ethyl propanoate and to develop detailed chemical kinetic mechanisms for their oxidation to enhance our knowledge of the oxidation processes of biodiesel fuels.

2. Experimental Section

The steel shock tube consists of a large but short (52 cm diameter and 63 cm long) driver section coupled via a 10 cm long transition piece to the test section which is 622 cm long and 10.24 cm internal diameter. Pressure transducers (PCB Piezotronics, model 113A21) were set into the final 50 cm of the test section and were used to measure the incident shock velocity with the aid of three universal time counters (Fluke/Phillips PM 6666). To allow for shock attenuation, the shock velocity at the end wall was calculated by extrapolating the incident velocities to the endwall. Reflected-shock conditions were calculated, using the usual one-dimensional shock relations,[14] and the application GasEq,[15] from initial temperatures in the range 290−298 K, and initial pressures in the range 17−100 Torr.

A polycarbonate diaphragm was allowed to burst under pressure with the assistance of a cross-shaped cutting device that petaled the diaphragm. This ensured uniform bursting of the diaphragm and uniform shock front formation. This shock tube was fully characterized[16] in line with a previous account[17] and validated against recent experiments on n-heptane oxidation from the Stanford group.[18]

Test mixtures were prepared in a 35 L stainless steel tank using standard manometric methods. Gases were obtained from BOC Ireland Ltd.; helium CP Grade 99.999%, argon zero grade 99.998%, and oxygen research grade 99.985%. All gases were used without further purification. Methyl butanoate and ethyl propanoate were obtained from Aldrich Chemical Co. Ltd. and were determined to be 99.6% pure by GC analysis. To minimize the presence of atmospheric air in the sample, the liquid fuels were subjected to several freeze−pump−thaw degassing cycles before being used. Liquid fuel was incorporated into the mixing vessel by vaporization into the evacuated (10^{-6} Torr) mixing tank, and partial pressures were measured using a 100 Torr Baratron gauge to an accuracy of 0.01 Torr. Argon was added using a Wallace and Tiernan 800 Torr absolute pressure gauge. The exact composition of mixtures used during this study are shown in Table 1. Test gas mixtures were normally made up to a final pressure of 800 Torr and allowed to stand for 24 h or stirred for 2 h with a Teflon stirring bar to ensure homogeneity. From the resulting mix, initial pressures, p_1, varying from 17 to 100 Torr were used.

Emissions were observed using an end on detection diagnostic that consisted of a PDA55 (switchable gain, amplified silicon detector) located behind a 431 nm (for CH* emission) narrow bandpass filter with a spectral bandwidth of 10 nm. The filter and the PDA were aligned behind a quartz window located in the endwall.

A Kistler pressure transducer, mounted flush with the endwall, signaled the shock wave arrival at the endwall and the beginning of the ignition delay period. The end of the period was defined as the maximum rise in the rate of emission. The ignition delay time was defined as the time elapsed between the arrival of the shock wave at the endwall and the maximum rate of change of CH* emission.

3. Computational Model

All of the modeling computations in this study were carried out using the HCT modeling code.[19] The thermodynamic properties for the relevant radicals and stable parents were obtained using Benson's[20] group additivity method employing THERM[21] with updated H/C/O groups and bond dissociation groups taking into account the work of Lay et al.[22] and Sumathi and Green.[23] The NIST database[24] has been extensively used to help in the current analysis. When possible, the data employed here have been compared to, and are in excellent agreement with, that present in the NIST WebBook,[25] which is essentially a critical evaluation of available experimental data. The table of group values used to calculate the thermodynamic properties of the species in the ethyl propanoate submechanism is available from the authors.

The detailed kinetic mechanism for methyl butanoate oxidation is derived from the work of Fisher et al.[10] However, as this mechanism was published a numbers of years ago, there have been a number of changes made:

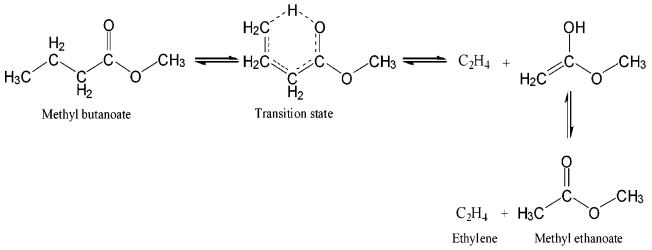

Figure 1. Six-centered unimolecular elimination for methyl butanoate producing methyl ethanoate and ethylene.

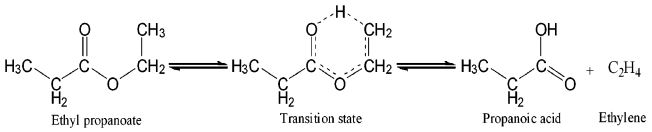

Figure 2. Six-centered unimolecular elimination for ethyl propanoate producing propanoic acid and ethylene.

•The H_2/O_2 submechanism has been replaced with that published recently by Ó Conaire et al.[26]

•The $R\dot{C}HC(=O)OCH_3$ bond strength has been reduced to 93.6 kcal mol^{-1} from 96.2 kcal mol^{-1} as published by Fisher et al. due to more recent calculations presented in ref 27.

•The rate constants for MB radical decomposition have been adjusted taking the work of Curran[28] on alkyl/alkoxyl radical decomposition into account.

•The high-pressure limit expression for unimolecular fuel decomposition reaction has been decreased by 66% (multiplied by 0.33).

•Unimolecular fuel decomposition reactions have been treated using quantum Rice−Ramsperger−Kassel theory based on the analysis using CHEMDIS developed by Bozzelli and Dean[29] to account for pressure falloff, and a Troe fit[30] generated to fit the data.

•A six-centered unimolecular elimination reaction that yields ethylene and methyl acetate was added with an activation energy of 68 kcal mol^{-1},[27] Figure 1.

Shock tube ignition delay times are extremely sensitive to the rates of unimolecular fuel decomposition. Thus, accounting for pressure falloff associated with this reaction class is the most significant change that we have made to the Fisher et al. mechanism to improve agreement. However, on making this change, predicted ignition delay times were still faster than experiment for all conditions. Thus, the high-pressure limit expressions were reduced by 66% relative to those developed by Fisher et al. to produce the current comparisons with experiment. The rate constant for the six-centered MB elimination reaction producing methyl ethanoate (through an enol−keto tautomerization) and ethylene, Figure 1, was estimated from the work of O'Neal and Benson[31] and Blades and Sandhu.[32] The addition of this reaction was found to contribute only about 1.0% to fuel consumption and thus has no significant role to play in fuel consumption under the conditions of this study. A full listing of this revised Fisher et al. mechanism is available for download at http://www.nuigalway.ie/chem/combust.htm#mecs. We have not included the detailed chemical kinetic mechanism for methyl butanoate in this paper as a large part has been published previously and our adjustments are relatively minor.

The ethyl propanoate submechanism was developed by analogy with methyl butanoate. Rate constants for ethyl propanoate unimolecular fuel decomposition and hydrogen atom abstractions are taken directly by analogy with methyl butanoate. However, a six-centered unimolecular elimination reaction producing propanoic acid and ethylene has been added, Figure 2. The activation energy of 50 kcal mol^{-1} for this reaction was taken from the associated work of El-Nahas et al.,[27] which is in good agreement with the value of 48.1 kcal mol^{-1} recommended by O'Neal and Benson[31] in their calculations and in reviewing the work of Blades and Sandhu.[32] The *A* factor is taken from the recommendation of O'Neal and Benson as the ab initio calculations of El-Nahas et al. do not account for the contribution of hindered rotors and as such the frequency factor is not accurately estimated. As with the updated methyl butanoate mechanism, the ethyl propanoate mechanism contains the recently published H_2/O_2 submechanism by Ó Conaire et al., and the unimolecular decomposition reactions have been treated to account for pressure falloff.

The ethylene submechanism is based on that which has been published previously by Curran et al.[33−36] for dimethyl ether oxidation and includes chemistry for species up to C_2. The rate constants for the important vinyl/oxygen reactions have been taken from Marinov et al.[37]

The propanoic acid submechanism has been developed in *this study* and is based on the work of Curran et al.[38,39] for *n*-heptane and iso-octane kinetic mechanism development. The rate constants used for primary hydrogen atom abstraction are those for primary hydrogen abstraction from an alkane. Rate constants for hydrogen atom abstraction of the "secondary" hydrogen atoms (i.e., $RCH_2(C=O)OH$) are taken to be identical to those of the similar hydrogen atom in methyl butanoate from the study of Fisher et al.[10] The rate constants for the decomposition reactions of propanoic acid to methyl radical and $\dot{C}H_2COOH$, and methyl ketene and water were taken from Doolan et al.[40] To achieve satisfactory agreement with experiment, we had to pay particular attention to the decomposition of the $CH_3\dot{C}HCOOH$ radical producing methyl ketene (CH_3CHCO) and a hydroxyl radical, and propenoic acid (C_2H_3COOH) and a $\dot{H}$ atom.

$$CH_3\dot{C}HCOOH \rightarrow CH_3CHCO + \dot{O}H$$

$$CH_3\dot{C}HCOOH \rightarrow C_2H_3COOH + \dot{H}$$

The rate constant for the addition of hydroxyl to methyl ketene was taken from Hatakeyama et al.[41] and that for the addition of $\dot{H}$ to propenoic acid from Curran[28] by analogy with $\dot{H}$ atom addition to propene. A listing of the ethyl propanoate submechanism is given in Table 3, and the complete mechanism is available in Chemkin format on the Combustion Research Centre's website.

Shock tube ignition delay times were simulated by assuming constant volume behind the reflected shock wave. However, our current mechanism does not include the chemistry for the electronically excited CH* species. Thus, to calculate an ignition delay time consistent with experiment, we use the recommendation of Horning et al.,[42] who found that the rate of emission can be inferred from the rate of production of CH*:

$$\dot{C}_2H + \dot{O} \rightarrow CH^* + CO$$

and defined the simulated ignition delay time as the time at which the maximum value of $[\dot{C}_2H] \times [\dot{O}]$ occurs.

4. Results and Discussion

Because ethyl propanoate undergoes a unimolecular elimination reaction to form propanoic acid and ethylene with a low activation energy barrier, it is pertinent to first test these

TABLE 3: Ethyl Propanoate Mechanism Rate Coefficients (cm^3 mol^{-1} s^{-1} cal^{-1})

	reaction	A	n	E_A
1.	EP = EP3J + H	2.33E+16	0.01	101400
	reverse	1.00E+14	0	0
	low-pressure limit	9.74E+103	−24.61	115400
	Troe values a = 0.87, T^{***} = 9.99E+09, T^{*} = 2.93E+01, T^{**} = 7.60E+07			
2.	EP = EP2J + H	3.18E+14	0.31	93330
	reverse	1.00E+14	0	0
	low-pressure limit	4.44E+125	−30.80	114000
	Troe values a = 0.96, T^{***} = 1.0E+10, T^{*} = 1.34, T^{**} = 6.70E+08			
3.	EP = EPEJ + H	2.01E+15	0.24	97550
	reverse	1.00E+14	0	0
	low-pressure limit	1.33E+113	−27.26	114100
	Troe values a = 8.41E−02, T^{***} = 3.62, T^{*} = 1.0E+10, T^{**} = 6.71E+09			
4.	EP = EPMJ + H	3.22E+17	−0.38	102900
	reverse	1.00E+14	0	0
	low-pressure limit	9.74E+103	−24.61	115400
	Troe values a = 0.87, T^{***} = 9.99E+09, T^{*} = 2.93E+01, T^{**} = 7.60E+07			
5.	EP = C_2H_5COOH + C_2H_4	4.00E+12	0.00	50000
	reverse	9.40E+02	2.25	34080
	low-pressure limit	1.88E+13	−1.03	11980
	Troe values a = 0.76, T^{***} = 1.0E+10, T^{*} = 1.74, T^{**} = 9.33E+09			
6.	EP = EE2J + CH_3	5.73E+23	−2.33	87740
	reverse	2.0E+17	−1.36	380
	low-pressure limit	4.35E+14	0.82	63570
	Troe values a = 0.17, T^{***} = 5.71E+03, T^{*} = 4.05E+01, T^{**} = 6.71E+09			
7.	EP = C_2H_5OCO + C_2H_5	2.63E+27	−3.23	94690
	reverse	3.15E+16	−1.07	3470
	low-pressure limit	7.72E+18	−0.27	71920
	Troe values a = 0.63, T^{***} = 8.82E+09, T^{*} = 1.62E+03, T^{**} = 7.60E+07			
8.	EP = C_2H_5CO + C_2H_5O	1.65E+24	−2.04	100200
	reverse	9.87E+16	−1.24	1934
	low-pressure limit	1.36E+16	0.76	78320
	Troe values a = 0.74, T^{***} = 7.33E+09, T^{*} = 2.12E+03, T^{**} = 6.71E+09			
9.	EP = $C_2H_5CO_2$ + C_2H_5	5.73E+25	−2.76	92110
	reverse	5.85E+13	−0.28	1630
	low-pressure limit	9.71E+16	0.28	68840
	Troe values a = 0.45, T^{***} = 1.26E+03, T^{*} = 4.68E+09, T^{**} = 1.79E+09			
10.	EP = MPMJ + CH_3	3.39E+21	−1.58	92090
	reverse	1.83E+14	−0.59	−60
	low-pressure limit	5.67E+12	1.46	68820
	Troe values a = 0.41, T^{***} = 1.52E+03, T^{*} = 4.84E+09, T^{**} = 9.33E+09			
11.	EP + O_2 = EP3J + HO_2	3.00E+13	0	52290
	reverse	2.70E+11	−0.08	−239
12.	EP + O_2 = EP2J + HO_2	2.00E+13	0	44300
	reverse	1.32E+13	−0.39	−159
13.	EP + O_2 = EPEJ + HO_2	2.00E+13	0	48200
	reverse	2.01E+12	−0.31	−479
14.	EP + O_2 = EPMJ + HO_2	3.00E+13	0	52290
	reverse	1.95E+10	0.30	−1759
15.	EP + H = EP3J + H_2	6.66E+05	2.54	6756
	reverse	1.14E+03	2.81	8916
16.	EP + H = EP2J + H_2	2.52E+14	0	7300
	reverse	3.16E+13	−0.04	1753
17.	EP + H = EPEJ + H_2	1.20E+06	2.40	2583
	reverse	2.39E+04	2.43	8593
18.	EP + H = EPMJ + H_2	6.66E+05	2.54	6756
	reverse	8.26E+01	3.19	7396
19.	EP + O = EP3J + OH	9.81E+05	2.43	4750
	reverse	8.82E+02	2.68	5498
20.	EP + O = EP2J + OH	2.20E+13	0	3280
	reverse	1.45E+12	−0.06	12100
21.	EP + O = EPEJ + OH	7.66E+05	2.41	1140
	reverse	7.97E+03	2.42	5738
22.	EP + O = EPMJ + OH	9.81E+05	2.43	4750
	reverse	6.38E+01	3.06	3978
23.	EP + OH = EP3J + H_2O	5.28E+09	0.97	1586
	reverse	9.63E+07	1.13	18640
24.	EP + OH = EP2J + H_2O	1.15E+11	0.51	63
	reverse	1.53E+11	0.37	25180
25.	EP + OH = EPEJ + H_2O	1.15E+11	0.51	63
	reverse	2.42E+10	0.44	20960
26.	EP + OH = EPMJ + H_2O	5.28E+09	0.97	1586
	reverse	6.96E+06	1.52	17120
27.	EP + CH_3 = EP3J + CH_4	4.53E−01	3.65	7154
	reverse	7.08E−01	3.47	10850

TABLE 3: (Continued)

	reaction	*A*	*n*	E_A
28.	EP + CH_3 = EP2J + CH_4	2.00E+11	0	7900
	reverse	2.29E+13	−0.48	19670
29.	EP + CH_3 = EPEJ + CH_4	1.20E−09	6.36	893
	reverse	2.18E−08	5.95	8443
30.	EP + CH_3 = EPMJ + CH_4	4.53E−01	3.65	7154
	reverse	5.13E−02	3.86	9334
31.	EP + HO_2 = EP3J + H_2O_2	2.38E+04	2.55	16490
	reverse	2.36E+04	2.12	2649
32.	EP + HO_2 = EP2J + H_2O_2	4.32E+12	0	14400
	reverse	3.14E+14	−0.73	8629
33.	EP + HO_2 = EPEJ + H_2O_2	7.22E+03	2.55	10530
	reverse	8.29E+04	1.89	539
34.	EP + HO_2 = EPMJ + H_2O_2	2.38E+04	2.55	16490
	reverse	1.71E+03	2.51	1129
35.	EP + CH_3O_2 = EP3J + CH_3O_2H	2.38E+04	2.55	16490
	reverse	4.59E+05	1.68	1054
36.	EP + CH_3O_2 = EP2J + CH_3O_2H	4.32E+12	0	14400
	reverse	6.11E+15	−1.18	7034
37.	EP + CH_3O_2 = EPEJ + CH_3O_2H	7.22E+03	2.55	10530
	reverse	1.61E+06	1.45	−1056
38.	EP + CH_3O_2 = EPMJ + CH_3O_2H	2.38E+04	2.55	16490
	reverse	3.32E+04	2.06	−466
39.	EP + C_2H_5 = EP3J + C_2H_6	4.52E−01	3.65	9141
	reverse	8.39E+00	3.23	9071
40.	EP + C_2H_5 = EP2J + C_2H_6	2.00E+11	0	7900
	reverse	2.72E+14	−0.72	15900
41.	EP + C_2H_5 = EPEJ + C_2H_6	1.08E+00	3.46	5962
	reverse	2.33E+02	2.81	9742
42.	EP + C_2H_5 = EPMJ + C_2H_6	4.52E−01	3.65	9141
	reverse	6.07E−01	3.62	7551
43.	EP + C_2H_3 = EP3J + C_2H_4	3.02E+02	3.30	10500
	reverse	1.64E+03	3.06	20420
44.	EP + C_2H_3 = EP2J + C_2H_4	4.00E+11	0	14300
	reverse	1.59E+14	−0.54	32290
45.	EP + C_2H_3 = EPEJ + C_2H_4	1.81E+00	3.46	2611
	reverse	1.14E+02	2.99	16380
46.	EP + C_2H_3 = EPMJ + C_2H_4	3.02E+02	3.30	10500
	reverse	1.18E+02	3.45	18900
47.	EP + CH_3O = EP3J + CH_3OH	2.17E+11	0	6458
	reverse	7.98E+09	0.05	8845
48.	EP + CH_3O = EP2J + CH_3OH	3.80E+10	0	2800
	reverse	1.03E+11	−0.25	13260
49.	EP + CH_3O = EPEJ + CH_3OH	4.58E+10	0	2873
	reverse	1.95E+10	−0.18	9110
50.	EP + CH_3O = EPMJ + CH_3OH	2.17E+11	0	6458
	reverse	3.05E+09	0.23	9463
51.	EP3J = C_2H_4 + C_2H_5OCO	8.83E+15	−0.67	35550
	reverse	1.32E+04	2.48	6130
52.	EP2J = EPMJ	2.32E+15	−1.26	19100
	reverse	7.34E+12	−0.67	11270
53.	EP2J = CH_3CHCO + C_2H_5O	2.79E+22	−2.31	45660
	reverse	5.00E+11	0	−1000
54.	EP2J = EP1D + H	1.32E+14	−0.16	40890
	reverse	4.24E+11	0.51	1230
55.	EPEJ = CH_3CHO + C_2H_5CO	1.13E+21	−1.73	40550
	reverse	2.00E+12	0	24000
56.	EPMJ = C_2H_4 + $C_2H_5CO_2$	2.33E+14	−0.20	32970
	reverse	1.32E+04	2.48	6130
57.	EP1D = C_2H_3 + C_2H_5OCO	4.28E+22	−1.66	107800
	reverse	1.00E+13	0	0
58.	EP1D = C_2H_3CO + C_2H_5O	1.38E+23	−1.83	90230
	reverse	2.00E+13	0	0
59.	EP1D = MP1DMJ + CH_3	2.52E+20	−1.02	92230
	reverse	1.00E+13	0.00	0
60.	EP1D + O_2 = EP1DEJ + HO	2.00E+13	0.00	48200
	reverse	1.77E+12	−0.29	−479
61.	EP1D + O_2 = EP1DMJ + HO_2	3.00E+13	0.00	52290
	reverse	1.14E+10	0.38	−1819
62.	EP1D + H = EP1DEJ + H_2	1.20E+06	2.40	2583
	reverse	2.03E+04	2.46	8593
63.	EP1D + H = EP1DMJ + H_2	6.66E+05	2.54	6756
	reverse	4.80E+01	3.27	7336
64.	EP1D + O = EP1DEJ + OH	7.66E+05	2.41	1140
	reverse	6.77E+03	2.44	5738

TABLE 3: (Continued)

	reaction	*A*	*n*	E_A
65.	EP1D + O = EP1DMJ + OH	9.81E+05	2.43	4750
	reverse	3.71E+01	3.14	3918
66.	EP1D + OH = EP1DEJ + H_2O	1.15E+11	0.51	63
	reverse	2.05E+10	0.46	20960
67.	EP1D + OH = EP1DMJ + H_2O	5.28E+09	0.97	1586
	reverse	4.05E+06	1.59	17060
68.	EP1D + CH_3 = EP1DEJ + CH_4	1.20E−09	6.36	893
	reverse	1.84E−08	5.97	8443
69.	EP1D + CH_3 = EP1DMJ + CH_4	4.53E−01	3.65	7154
	reverse	2.98E−02	3.93	9274
70.	EP1D + HO_2 = EP1DEJ + H_2O_2	7.22E+03	2.55	10530
	reverse	7.04E+04	1.91	539
71.	EP1D + HO_2 = EP1DMJ + H_2O_2	2.38E+04	2.55	16490
	reverse	9.93E+02	2.58	1069
72.	EP1D + CH_3O_2 = EP1DEJ + CH_3O_2H	7.22E+03	2.55	10530
	reverse	1.37E+06	1.47	−1056
73.	EP1D + CH_3O_2 = EP1DMJ + CH_3O_2H	2.38E+04	2.55	16490
	reverse	1.93E+04	2.14	−526
74.	EP1D + C_2H_5 = EP1DEJ + C_2H_6	1.08E+00	3.46	5962
	reverse	1.98E+02	2.83	9742
75.	EP1D + C_2H_5 = EP1DMJ + C_2H_6	4.52E−01	3.65	9141
	reverse	3.53E−01	3.69	7491
76.	EP1D + C_2H_3 = EP1DEJ + C_2H_4	1.81E+00	3.46	2611
	reverse	9.64E+01	3.01	16380
77.	EP1D + C_2H_3 = EP1DMJ + C_2H_4	3.02E+02	3.30	10500
	reverse	6.89E+01	3.52	18840
78.	EP1D + CH_3O = EP1DEJ + CH_3OH	4.58E+10	0	2873
	reverse	1.66E+10	−0.16	9110
79.	EP1D + CH_3O = EP1DMJ + CH_3OH	2.17E+11	0	6458
	reverse	6.31E+08	0.39	8993
80.	EP1DEJ = CH_3CHO + CH_2CHCO	2.42E+23	−2.69	33270
	reverse	2.00E+12	0	24000
81.	EP1DMJ = C_2H_4 + $C_2H_3CO_2$	1.50E+12	0.44	32020
	reverse	1.32E+04	2.48	6130
82.	$C_2H_3CO_2$ = C_2H_3 + CO_2	1.00E+13	0	10000
	reverse	4.01E+05	−0.85	10960
83.	C_2H_5OCO = C_2H_5O + CO	5.06E+14	0.17	25520
	reverse	1.55E+06	2.02	5730
84.	C_2H_5OCO = C_2H_5 + CO_2	1.81E+16	−0.56	20170
	reverse	4.76E+07	1.54	34700
85.	EE2J = CH_2CO + C_2H_5O	9.36E+19	−1.88	56420
	reverse	1.00E+11	0	12900
86.	MPMJ = CH_2O + C_2H_5CO	7.95E+20	−1.82	44530
	reverse	2.00E+12	0	24000
87.	MP1DMJ = CH_2O + C_2H_3CO	2.42E+23	−2.82	36410
	reverse	2.00E+12	0	24000
88.	C_2H_5COOH = CH_3CHCO + H_2O	7.08E+12	0	70510
	reverse	1.31E+05	1.48	38300
89.	C_2H_5COOH = CH_3 + CH2COOH	3.98E+15	0	88430
	reverse	2.03E+09	0.89	1352
90.	C_2H_5COOH = C_2H_5 + HOCO	5.65E+21	−2.05	95950
	reverse	1.51E+11	0	4810
91.	C_2H_5COOH = C_2H_5CO + OH	1.09E+18	−0.12	108900
	reverse	5.00E+13	0	0
92.	C_2H_5COOH + O_2 = CH_2CH_2COOH + HO_2	3.00E+13	0	52290
	reverse	4.49E+10	0.25	−59
93.	C_2H_5COOH + O_2 = $CH_3CHCOOH$ + HO_2	2.00E+13	0	44300
	reverse	1.21E+13	−0.38	−189
94.	C_2H_5COOH + H = CH_2CH_2COOH + H_2	6.66E+05	2.54	6756
	reverse	1.90E+02	3.14	9096
95.	C_2H_5COOH + H = $CH_3CHCOOH$ + H_2	2.54E+14	0	7300
	reverse	2.93E+13	−0.03	17500
96.	C_2H_5COOH + O = CH_2CH_2COOH + OH	9.81E+05	2.43	4750
	reverse	1.47E+02	3.00	5678
97.	C_2H_5COOH + O = $CH_3CHCOOH$ + OH	2.20E+13	0	3280
	reverse	1.33E+12	−0.05	12070
98.	C_2H_5COOH + OH = CH_2CH_2COOH + H_2O	5.28E+09	0.97	1586
	reverse	1.60E+07	1.46	18820
99.	C_2H_5COOH + OH = $CH_3CHCOOH$ + H_2O	1.15E+11	0.51	63
	reverse	1.41E+11	0.38	25160
100.	C_2H_5COOH + CH_3 = CH_2CH_2COOH + CH_4	4.53E−01	3.65	7154
	reverse	1.18E−01	3.80	11030
101.	C_2H_5COOH + CH_3 = $CH_3CHCOOH$ + CH_4	2.00E+11	0.00	7900
	reverse	2.10E+13	−0.47	19640

TABLE 3: (Continued)

	reaction	*A*	*n*	E_A
102.	$C_2H_5COOH + HO_2 = CH_2CH_2COOH + H_2O_2$	2.38E+04	2.55	16490
	reverse	3.93E+03	2.45	2829
103.	$C_2H_5COOH + HO_2 = CH_3CHCOOH + H_2O_2$	4.32E+12	0	14400
	reverse	2.88E+14	−0.72	8599
104.	$C_2H_5COOH + CH_3O_2 = CH_2CH_2COOH + CH_3O_2H$	2.38E+04	2.55	16490
	reverse	7.64E+04	2.01	1234
105.	$C_2H_5COOH + CH_3O_2 = CH_3CHCOOH + CH_3O_2H$	4.32E+12	0	14400
	reverse	5.61E+15	−1.17	7004
106.	$C_2H_5COOH + CH_3O = CH_2CH_2COOH + CH_3OH$	2.17E+11	0	6458
	reverse	1.33E+09	0.38	9025
107.	$C_2H_5COOH + CH_3O = CH_3CHCOOH + CH_3OH$	3.80E+10	0	2800
	reverse	9.40E+10	−0.24	13230
108.	$C_2H_5COOH + C_2H_5 = CH_2CH_2COOH + C_2H_6$	4.52E−01	3.65	9140
	reverse	1.40E+00	3.56	9250
109.	$C_2H_5COOH + C_2H_5 = CH_3CHCOOH + C_2H_6$	2.00E+11	0	7900
	reverse	6.35E+13	−0.54	15590
110.	$C_2H_5COOH + C_2H_3 = CH_2CH_2COOH + C_2H_4$	3.02E+02	3.30	10500
	reverse	6.25E+02	3.23	20560
111.	$C_2H_5COOH + C_2H_3 = CH_3CHCOOH + C_2H_4$	4.00E+11	0	14300
	reverse	3.71E+13	−0.37	31980
112.	$CH_2CH_2COOH = C_2H_4 + HOCO$	4.22E+14	−0.32	34860
	reverse	1.32E+04	2.48	6130
113.	$CH_3CHCOOH = CH_3CHCO + OH$	3.05E+21	−1.61	57300
	reverse	4.58E+13	0	0
114.	$CH_3CHCOOH = C_2H_3COOH + H$	6.16E+13	−0.13	42240
	reverse	2.50E+11	0.51	2620
115.	$CH_2COOH = CH_2CO + OH$	4.64E+18	−1.28	53860
	reverse	2.60E+12	0	−614
116.	$C_2H_3COOH = C_2H_3 + HOCO$	3.75E+21	−1.89	112900
	reverse	1.51E+11	0	4810
117.	$C_2H_3COOH = C_2H_3CO + OH$	5.21E+20	−1.16	100900
	reverse	5.00E+13	0	0
118.	$C_2H_5CO_2 = C_2H_5 + CO_2$	4.40E+15	0	10500
	reverse	1.36E+08	1.78	24290
119.	$CH_2CHCO + OH = C_2H_4 + CO_2$	1.00E+12	0	0
	reverse	2.26E+11	0.80	102900
120.	$CH_2CHCO + HO_2 = C_2H_3 + CO_2 + OH$	6.03E+09	0	7949
	reverse	0.00E+00	0	0
121.	$CH_2CHCO + CH_3O_2 = C_2H_3 + CO_2 + CH_3O$	3.97E+11	0	17050
	reverse	0.00E+00	0	0

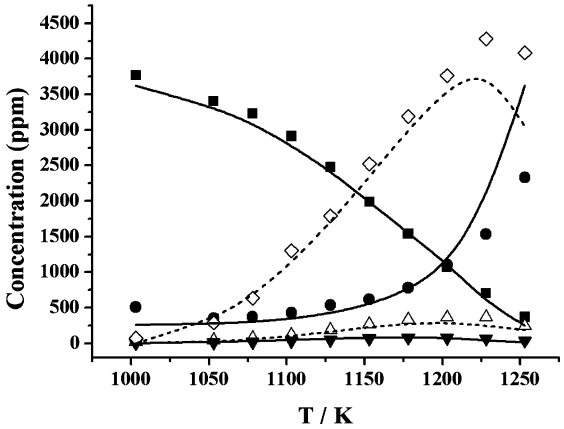

Figure 3. Species concentrations during ethylene oxidation between 1003 and 1253 K at 1 atm: (■) C_2H_4; (◇) CO; (●) CO_2; (△) H_2; (▼) CH_4. Symbols are experimental results; lines are model predictions. The dashed line corresponds to the open symbols.

submechanisms, which are important subsets of the ethyl propanoate oxidation system.

The ethylene submechanism has been used to simulate experimental results for ethylene obtained in two distinct jet-stirred reactors,[43,44] Figures 3 and 4, and in a shock tube,[45] Figure 5. Model simulations are in good agreement with experimental results and show that the chemistry producing intermediate species is reliable, Figures 3 and 4. Predicted ignition delay times are in reasonable agreement, with the model slower than experiment at high temperatures, Figure 5.

There are very little data available for propanoic acid consumption. Doolan et al.[40] studied the thermal decomposition (pyrolysis) of propanoic acid diluted in argon in a single-pulse shock tube in the temperature range 1100−1500 K and over the pressure range 14−18 atm. Fuel, intermediate, and product species concentration profiles were reported as a function of reflected-shock temperature. Comparisons of model predictions versus experimental results are shown in Figure 6. It is evident that the model captures correctly the consumption of propanoic acid as a function of temperature, in addition to the evolution of the major product species ethylene and carbon monoxide, Figure 6a. In addition, predicted profiles for carbon dioxide, acetylene, and methane are in reasonably good agreement with experimental results, Figure 6b.

Shock tube ignition delay times for EP/O_2/Ar mixtures were measured behind reflected shock waves over the temperature range 1140−1675 K, at reflected-shock pressures of 1.0 and 4.0 atm, and at equivalence ratios, ϕ, of 0.25, 0.5, 1.0, and 1.5, Figures 7 and 8. These figures show the experimental results (points) together with the model-simulated ignition delay times (lines). The data at both 1.0 atm (Figure 7) and 4.0 atm (Figure 8) show that as the EP concentration is increased from 1.0% (ϕ = 1.0) to 1.5% (ϕ = 1.5), with the O_2 concentration constant at 6.5%, the ignition delay times *increased*. This observation is in agreement with previous studies of hydrocarbons.[14] Increasing

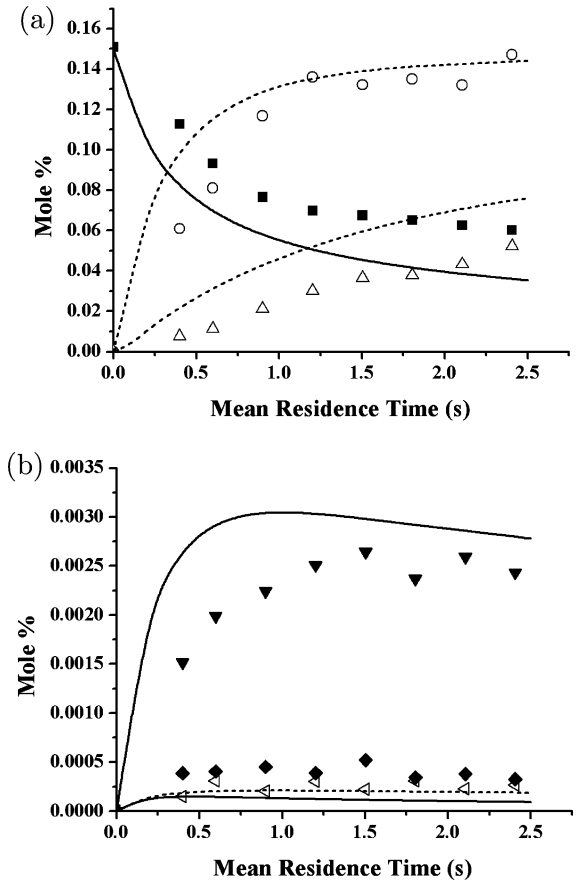

Figure 4. Oxidation in the high-pressure jet-stirred reactor of the mixture $C_2H_4/O_2/N_2$ (0.15%, 0.60%, 99.25%) at 10 atm and 888 K. (a) Key: (■) C_2H_4; (○) CO; (△) CO_2. (b) Key: (▼) CH_4; (◆) C_2H_6; (△) C_2H_2. Symbols are experimental results; lines are model predictions. The dashed line corresponds to the open symbols.

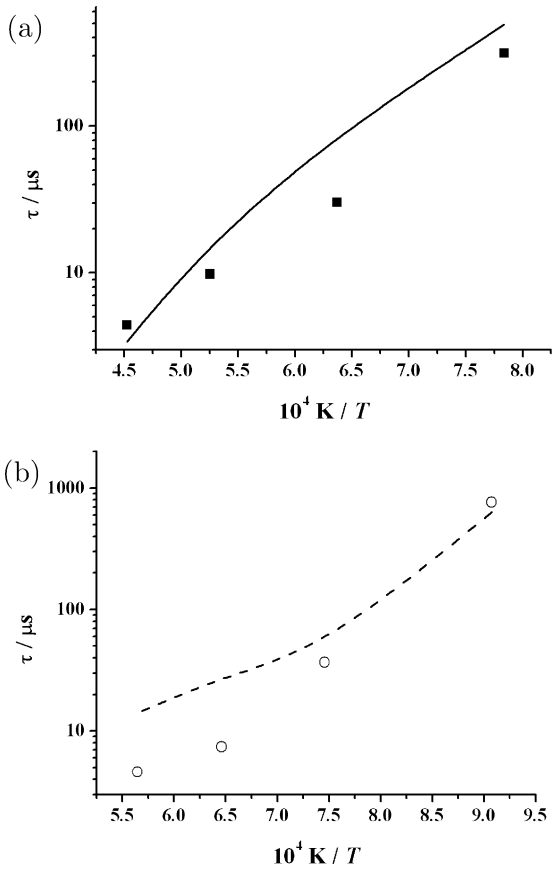

Figure 5. Shock tube ignition delay times in Ar mixtures between 1100 and 2210 K and 1.3 and 3.4 atm: (a) 1.0% C_2H_4, 3.0% O_2, 96.0% Ar; (b) 6.25% C_2H_4, 18.75% O_2, 75.0% Ar. Symbols are experimental results; lines are model predictions.

the oxygen concentration from 6.5% ($\phi = 1.0$), through 13.0% ($\phi = 0.5$), to 26.0% ($\phi = 0.25$), with a constant EP concentration of 1.0%, led to a significant *reduction* in delay times. This negative power dependence of oxygen is also in accordance with previous work.[14] The magnitude of the enhancing effect of oxygen is much more pronounced than is the inhibiting effect of the fuel concentration. This observation is also in agreement with previous studies of hydrocarbons. The concentration of argon in all three mixtures was essentially constant and so did not influence the delay times. Model-predicted ignition delay times are in good agreement with those measured and accurately capture the influence of fuel and oxygen concentration, Figures 7 and 8.

Ignition delay times obtained for a 1.0% EP/6.5% O_2 stoichiometric ($\phi = 1.0$) mixture, over the temperature range 1140−1675 K, at pressures of 1.0 and 4.0 atm, are shown in Figure 9, together with model predictions. The ignition delay times decrease as the reflected-shock pressure is increased from 1.0 to 4.0 atm, in agreement with most studies carried out to date[14] on hydrocarbons. The ignition delay times simulated using the EP mechanism, in conjunction with the HCT program, are in very good agreement with those measured experimentally and accurately capture the pressure dependence, Figure 9.

4.1. Rate of Production Analysis. To understand the chemistry of ethyl propanoate oxidation, a rate of production analysis was carried out using a stoichiometric mixture of 1.0% EP, 6.5% O_2 in 92.5% Ar, at a reflected-shock pressure of 1.0 atm and at 1200 K. A condition of 50% fuel consumed was chosen corresponding to a time of 282 μs. At first glance, the oxidation of ethyl propanoate looks relatively simple, Figure 10. This simulation shows that nearly all of the fuel reacts through a six-centered unimolecular elimination channel to form ethylene and propanoic acid with the further oxidation of these products subsequently controlling the ignition process. Indeed, under both fuel-rich and stoichiometric conditions this is effectively what happens.

$$C_2H_5C(O)OC_2H_5 \xrightarrow{96\%} C_2H_5COOH + C_2H_4$$

$$C_2H_5C(O)OC_2H_5 + \dot{H} \xrightarrow{2\%} EP2J + H_2$$

$$C_2H_5C(O)OC_2H_5 + \dot{H} \xrightarrow{1\%} EPEJ + H_2$$

$$C_2H_5C(O)OC_2H_5 + \dot{R} \xrightarrow{1\%} EP3J + RH$$

Due to the low activation energy barrier of 50.0 kcal mol^{-1}, this elimination reaction accounts for approximately 96% of the fuel breakdown with only than 4% undergoing H-atom abstraction reactions. (R = Ḣ, ȮH, and Ȯ). It can be clearly seen in Figure 10 that all of the fuel has disappeared (~750 μs) long before the ignition event takes place (1565 μs), with ethylene and propanoic acid effectively behaving as the fuel.

To further understand the chemistry of oxidation, the evolution of both ethylene and propanoic acid has been examined. In the following equation arrays, the values over the arrows correspond to the percentage contribution of that reaction to the overall consumption of the species.

Figure 10 shows that the ethylene concentration reaches a maximum at 1055 μs. Its concentration has decreased by 20% below this maximum at 1424 μs. At this time the principal reactions involved in the consumption of ethylene are

$$C_2H_4 + \dot{O}H \xrightarrow{35\%} \dot{C}_2H_3 + H_2O$$

$$C_2H_4 + \dot{H} \xrightarrow{30\%} \dot{C}_2H_3 + H_2$$

$$C_2H_4 + \dot{O} \xrightarrow{20\%} \dot{C}H_3 + HCO$$

$$C_2H_4 + \dot{O} \xrightarrow{12\%} \dot{C}H_2CHO + \dot{H}$$

It will be shown in the sensitivity analysis later that the two reactions producing vinyl are the most important in the oxidation of ethylene.

Figure 10 also shows that while the propanoic acid concentration reaches a maximum at approximately 560 μs, its concentration decreases 20% below this maximum at a time of 865 μs. At this time, propanoic acid undergoes hydrogen abstraction reactions, principally by $\dot{O}H$ and $\dot{H}$ to form two radicals, $CH_3\dot{C}HCOOH$ and $\dot{C}H_2CH_2COOH$, which then produce methyl ketene, hydroxyl, and hydrocarboxyl radicals and ethylene.

$$C_2H_5COOH + \dot{H} \xrightarrow{43\%} CH_3\dot{C}HCOOH + H_2$$

$$C_2H_5COOH + \dot{O}H \xrightarrow{26\%} CH_3\dot{C}HCOOH + H_2O$$

$$C_2H_5COOH + \dot{O}H \xrightarrow{16\%} \dot{C}H_2CH_2COOH + H_2O$$

$$C_2H_5COOH + \dot{H} \xrightarrow{9\%} \dot{C}H_2CH_2COOH + H_2$$

$$CH_3\dot{C}HCOOH \xrightarrow{59\%} C_2H_3COOH + \dot{H}$$

$$CH_3\dot{C}HCOOH \xrightarrow{41\%} CH_3CHCO + \dot{O}H$$

$$\dot{C}H_2CH_2COOH \xrightarrow{100\%} C_2H_4 + HO\dot{C}{=}O$$

Under fuel-lean conditions ($\phi = 0.25$), at 1200 K, 1 atm, and at 50% fuel consumed, reaction rate analysis shows that 57% of ethyl propanoate molecules decompose to produce ethylene and propanoic acid with 43% now undergoing hydrogen atom abstraction reactions to produce fuel-radical species, Figure 11. This increase in hydrogen atom abstraction (relative to molecular elimination) has a significant influence on the overall reactivity of the system.

$$C_2H_5C(O)OC_2H_5 \xrightarrow{57\%} C_2H_5COOH + C_2H_4$$

$$C_2H_5C(O)OC_2H_5 + \dot{R} \xrightarrow{15\%} EP2J + RH$$

$$C_2H_5C(O)OC_2H_5 + \dot{R} \xrightarrow{15\%} EPEJ + RH$$

The two main radicals formed are EP2J ($CH_3\dot{C}HC(O)OCH_2CH_3$) and EPEJ ($CH_3CH_2C(O)O\dot{C}HCH_3$). The decomposition of EP2J can be seen in Figure 12 and is described in section 4.3. EPEJ undergoes β-scission to produce acetaldehyde and propanal radical, which in turn decomposes to produce carbon monoxide and ethyl radical.

$$EPEJ \xrightarrow{100\%} CH_3CHO + C_2H_5\dot{C}O$$

$$C_2H_5\dot{C}O \xrightarrow{100\%} \dot{C}_2H_5 + CO$$

$$\dot{C}_2H_5 \xrightarrow{83\%} C_2H_5 + \dot{H}$$

Due to the greater concentration of molecular oxygen, and the corresponding increase in the rate of $\dot{H} + O_2$, there is a significant increase in the concentration of $\dot{O}$ and $\dot{O}H$ radicals under lean conditions, resulting in an increased contribution of H-atom abstraction from the fuel relative to stoichiometric- and fuel-rich conditions.

The differing chemistry under fuel-lean conditions in comparison to stoichiometric and rich ones is highlighted in Figure 13. This figure shows the results of a simulation in which ethyl propanoate was replaced by the appropriate amount of ethylene and propanoic acid, with this mixture then used as the fuel. This simulation (dashed line) is compared to the ethyl propanoate experimental data at 1.0 atm at $\phi = 1.0$ and 0.25. Under stoichiometric conditions, the ethylene/propanoic acid mixture is more reactive throughout the temperature range, especially at lower temperatures. This can be linked to the fact that ethylene and propanoic acid take time to be produced from the decay of ethyl propanoate. When ethylene and propanoic acid are used as the original fuels, they can react immediately, thus explaining the shorter ignition delay. This effect is greatly reduced as the temperature increases due to the faster decomposition of ethyl propanoate at elevated temperatures. This confirms that, under these conditions, the fuel converts relatively quickly into ethylene and propanoic acid whereas all other reactions of ethyl

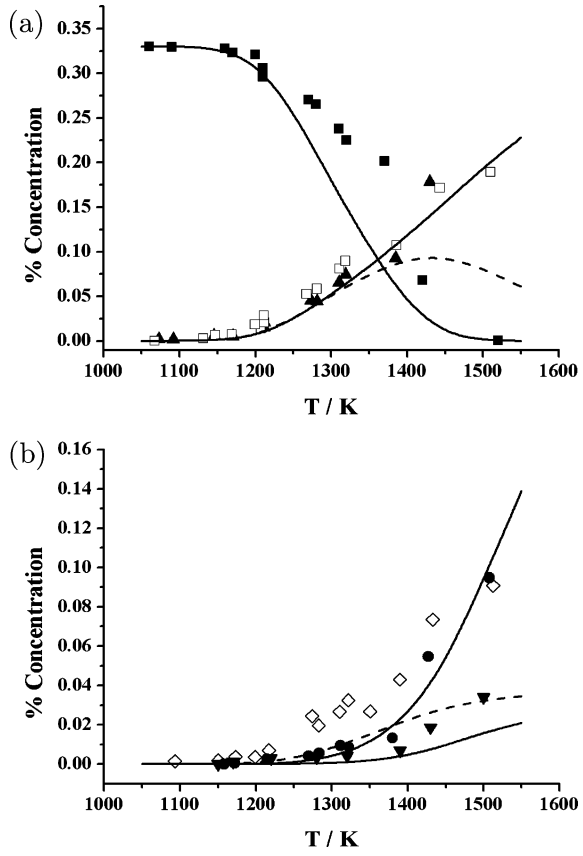

Figure 6. Concentration of indicated species as a function of reflected-shock temperature. The initial propanoic acid concentration was 0.33%. (a) Key: (■) C_2H_5COOH; (▲) CO; (□) C_2H_4. (b) Key: (◇) CO_2; (●) C_2H_2; (▼) CH_4. Symbols are experimental results; lines are model predictions. The dashed line corresponds to the open symbols.

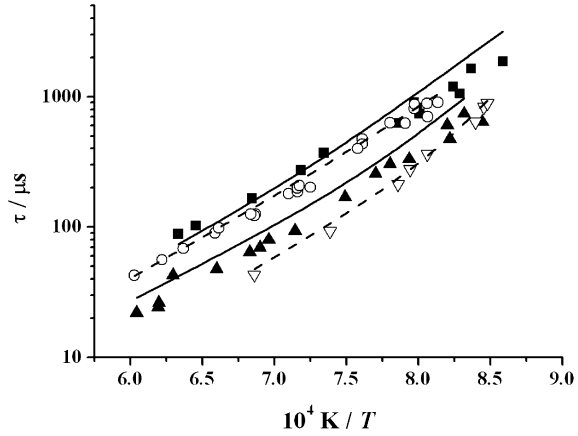

Figure 7. Ignition delay times for ethyl propanoate in Ar mixtures at 1 atm: (■) $\phi = 1.5$ (1.5% fuel, 6.5% O_2); (○) $\phi = 1.0$ (1.0% fuel, 6.5% O_2); (▲) $\phi = 0.5$ (1.0% fuel, 13.0% O_2); (▽) $\phi = 0.25$ (1.0% fuel, 26.0% O_2). Symbols are experimental results; lines are model predictions. The dashed line corresponds to the open symbols.

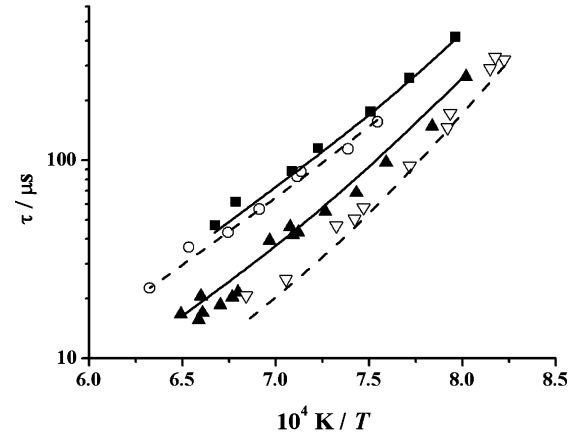

Figure 8. Ignition delay times for ethyl propanoate in Ar mixtures at 4 atm: (■) $\phi = 1.5$ (1.5% fuel, 6.5% O_2); (○) $\phi = 1.0$ (1.0% fuel, 6.5% O_2); (▲) $\phi = 0.5$ (1.0% fuel, 13.0% O_2); (▽) $\phi = 0.25$ (1.0% fuel, 26.0% O_2). Symbols are experimental results; lines are model predictions. The dashed line corresponds to the open symbols.

propanoate seem unimportant. Thus, the ignition delay time is controlled by the rate of oxidation of ethylene and propanoic acid. However, under lean conditions, assuming ethylene and propanoic acid to be the fuel does not capture the chemistry adequately, due to the importance of the ethyl propanoate radical species. The ethylene/propanoic acid mixture is once again considerably faster at lower temperatures but becomes too slow at higher temperatures. This is due to the reactions of vinyl, the major product from ethylene, with molecular oxygen. At lower temperatures, vinyl plus O_2 undergoes a chain-branching reaction, thus it has a large promoting effect on the reactivity of the system. As the temperature is increased, the most important reaction pathway for these moieties becomes a propagation step, thus reducing the reactivity of ethylene. At high temperatures and under lean conditions, the reactions of the fuel-radical species make an important contribution to the global reactivity, due to their increased production. This contribution is obviously not accounted for when assuming ethylene and propanoic acid to be the fuel; thus this simulation is too slow under these conditions. (The importance of vinyl plus O_2 chemistry is discussed more thoroughly in section 4.3) A comparative shock tube study of the mixture was considered, but we were unable to carry this out due to the low vapor pressure of propanoic acid, which is only 2.4 Torr at 20 °C.

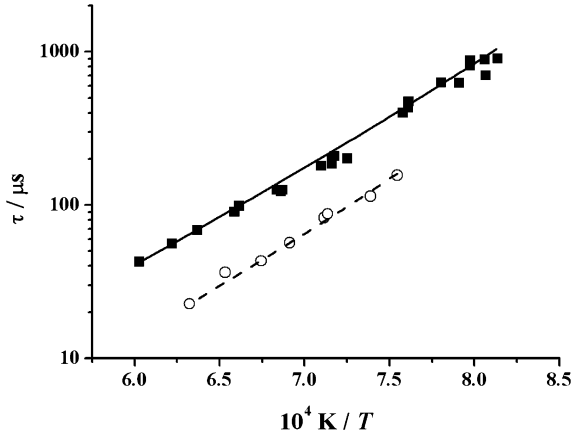

Figure 9. Effect of pressure on ignition delay at 1.0% fuel, $\phi = 1.0$: (■) EP at 1 atm: (○) EP at 4 atm. Symbols are experimental results; lines are model predictions. The dashed line corresponds to the open symbols.

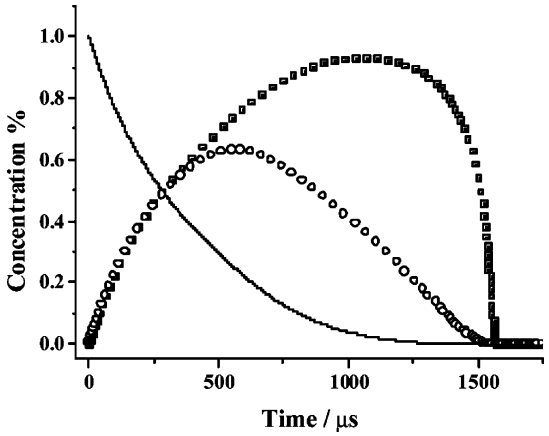

Figure 10. Ethyl propanoate decomposition to major products at 1200 K. Conditions: 1.0% EP, 6.5% O_2, 92.5% Ar. Key: (line) [EP]; (■) [C_2H_4]; (○) [C_2H_5COOH].

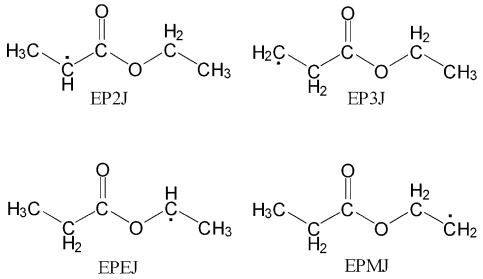

Figure 11. Nomenclature of ethyl propanoate fuel-radical species.

4.2. Methyl Butanoate versus Ethyl Propanoate. Comparisons of ignition delay times for methyl butanoate and ethyl propanoate mixtures at 1.0% fuel, 6.5% O_2 ($\phi = 1.0$) in argon, at 1.0 and 4 atm are shown in Figure 14. It is evident that ethyl propanoate is faster to ignite relative to methyl butanoate at both pressures, and this phenomenon is particularly prominent at lower temperatures. One may conclude that ethyl propanoate is always faster to ignite because of the six-centered unimolecular elimination reaction with its relatively low activation energy of approximately 50 kcal mol^{-1}. However, as depicted in Figure 10 for stoichiometric conditions, during the early stages of oxidation, ethyl propanoate is converted into ethylene and propanoic acid. It is the faster reactivity of these two species relative to methyl butanoate that is responsible for the faster reactivity of ethyl propanoate.

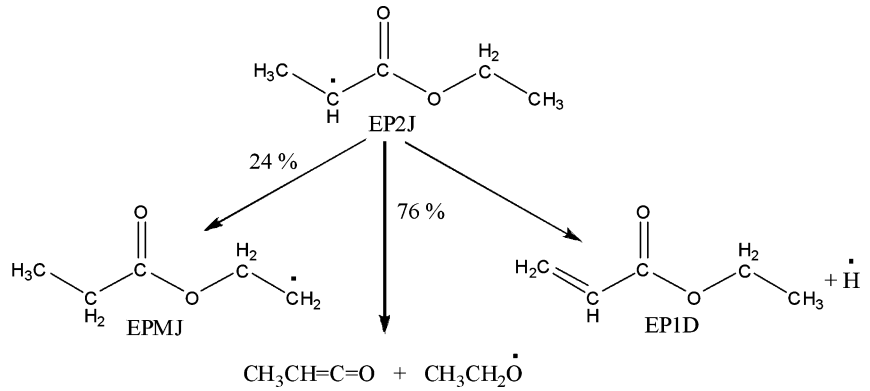

Figure 12. Decomposition pathway of fuel-radical species, EP2J. Percentages are the contribution of the reaction to the overall consumption of the species at $\phi = 0.25$ and 1 atm at 50% fuel consumption.

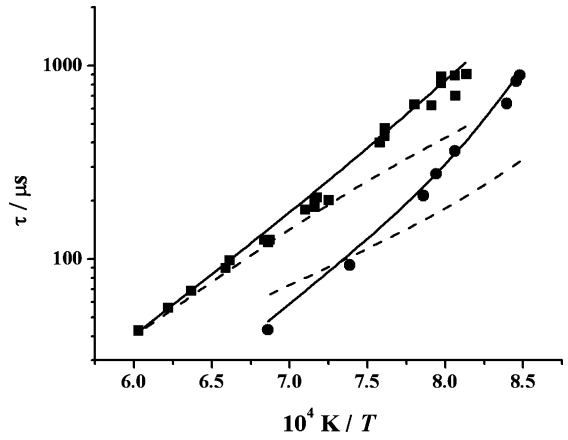

Figure 13. Ignition delay times for ethyl propanoate in Ar mixtures at 1 atm: (■) $\phi = 1.0$ (1.0% fuel, 6.5% O_2); (●) $\phi = 0.25$ (1.0% fuel, 26.0% O_2). Dashed lines are simulations using ethylene and propanoic acid as the fuel. The solid line corresponds to the baseline simulation.

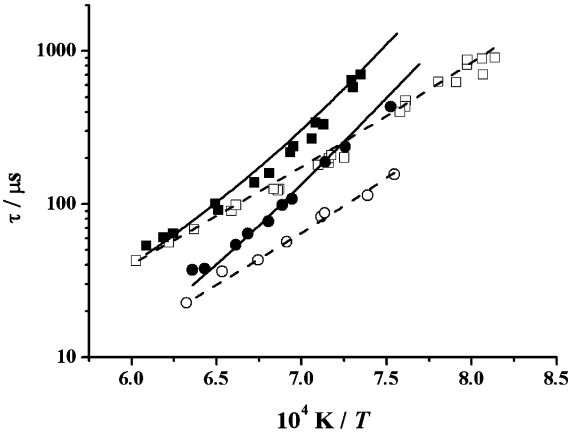

Figure 14. Comparison of fuel reactivity at 1.0% fuel, $\phi = 1.0$: (squares) 1 atm data; (circles) 4 atm data; (closed symbols) MB; (open symbols) EP. Symbols are experimental results; lines are model predictions. The dashed line corresponds to the open symbols.

4.3. Chemical Kinetic Mechanism: Sensitivity Analysis. The ethyl propanoate mechanism developed here contains 139 species and 786 reversible reactions. A detailed analysis was carried out to investigate the sensitivity of the principal reactions involved in its oxidation. This was performed by multiplying the rate constants of a particular reaction or reaction class by a factor of 2 (both forward and reverse rates) and then calculating the percent change in ignition delay time relative to the baseline simulation. A positive percent change indicates a longer ignition delay time and an overall decrease in reactivity, whereas a negative change indicates a shorter ignition delay time and an increase in reactivity. The analysis was carried out using a stoichiometric mixture of 1.0% EP, 6.5% O_2 in 92.5% Ar, at a reflected-shock pressure of 1.0 atm and temperatures of 1200 and 1600 K, respectively. A further study was carried out at 1200 K using a lean mixture of 1.0% EP and 26.0% O_2 in Ar ($\phi = 0.25$). This highlights how the relative importance of a reaction changes with equivalence ratio. The results of the analysis are shown in Figures 15 and 16.

The importance of the chain-branching reaction,

$$\dot{H} + O_2 \rightarrow \dot{O} + \dot{O}H$$

under all three conditions of this analysis is clearly shown in Figure 15. This reaction is one of the most important reactions in high-temperature auto-ignition. Under stoichiometric conditions, it is the most sensitive reaction at 1200 and 1600 K and is even more sensitive under lean conditions. The $\phi = 0.25$ mixture contains 26% O_2. With such a large concentration of oxygen present, increasing this reaction by a factor of 2 decreases the ignition delay time by more than 50%.

Figure 15 indicates the importance of reactions involving vinyl radicals and ethylene. Ethylene is present in large amounts as almost all of the ethyl propanoate decomposes to produce ethylene and propanoic acid, Figure 2. Ethylene in turn produces vinyl primarily through reactions with hydroxyl radical and atomic hydrogen. The reactions of vinyl and molecular oxygen, shown below, are extremely important to the overall reactivity.

$$\dot{C}_2H_3 + O_2 \rightarrow CH_2O + H\dot{C}O$$

$$\dot{C}_2H_3 + O_2 \rightarrow C_2H_2 + H\dot{O}_2$$

$$\dot{C}_2H_3 + O_2 \rightarrow \dot{C}H_2CHO + \dot{O}$$

The reaction producing formaldehyde and a formyl radical has a large positive sensitivity at 1200 K but has almost no effect on the ignition delay time at 1600 K. At 1200 K, when the rate for this reaction is doubled, it becomes the dominant pathway for the $\dot{C}_2H_3 + O_2$ reaction, thus decreasing the overall reactivity as it competes with the chain-branching reaction that forms $\dot{C}H_2$-CHO and $\dot{O}$ radicals. However, at 1600 K, its influence is unimportant because even with the rate doubled it is much slower than the other two channels and does not compete with them.

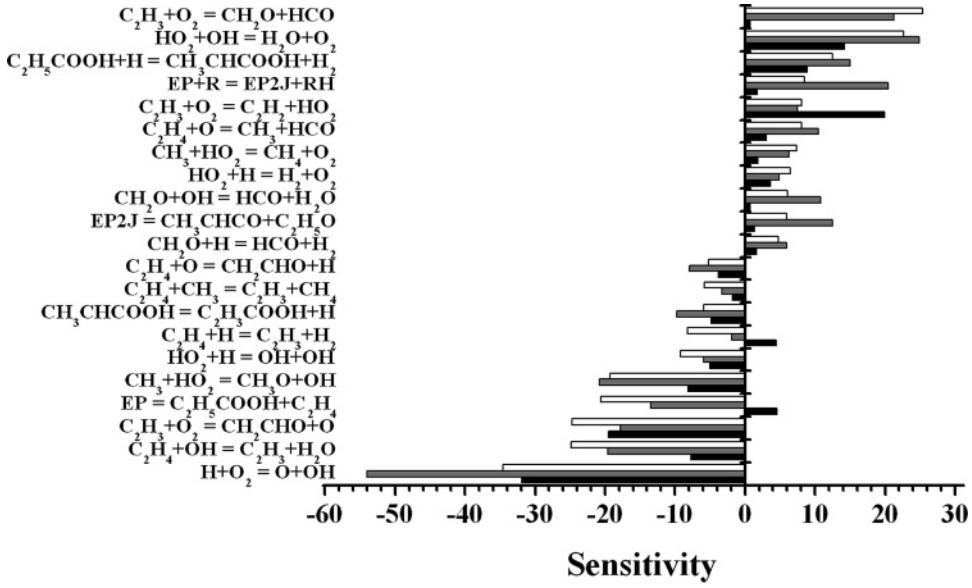

Figure 15. Sensitivity coefficients for 1% ethyl propanoate, 6.5% O_2, in argon at 1 atm: (white) 1200 K, $\phi = 1.0$; (gray) 1200 K, $\phi = 0.25$; (black) 1600 K, $\phi = 1.0$.

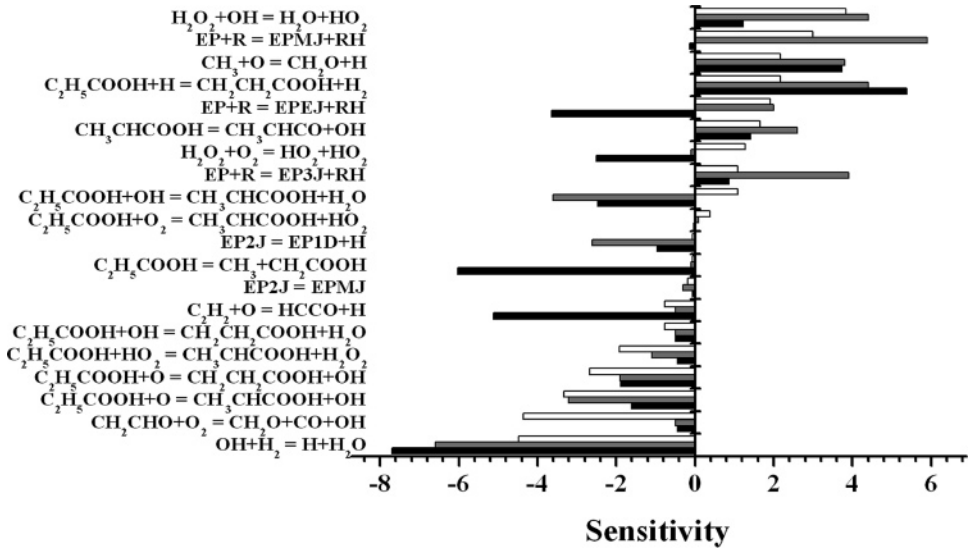

Figure 16. Sensitivity coefficients for 1% ethyl propanoate, 6.5% O_2, in argon at 1 atm: (white) 1200 K, $\phi = 1.0$; (gray) 1200 K, $\phi = 0.25$; (black) 1600 K, $\phi = 1.0$.

Figure 15 also shows the negative sensitivity coefficient for the reaction

$$C_2H_4 + \dot{O}H \rightarrow \dot{C}_2H_3 + H_2O$$

at 1200 K but has a much lower sensitivity coefficient at 1600 K. This again highlights the importance of vinyl/oxygen chemistry. The reaction between ethylene and a hydroxyl radical is the main source of vinyl radicals in the system. At low temperatures vinyl radicals predominantly undergo a chain-branching reaction with oxygen. Thus, increasing the production of vinyl radicals significantly increases the reactivity of the system. At higher temperatures, vinyl radicals react with molecular oxygen to form a stable acetylene molecule and a hydroperoxy radical. This is a propagation reaction not a chain-branching process, thus explaining the reduced effect of the reaction between ethylene and hydroxyl at 1600 K.

The other interesting result shown in Figure 15 is the negative sensitivity coefficient for the primary decomposition pathway of ethyl propanoate,

$$EP \rightarrow C_2H_5COOH + C_2H_4$$

at 1200 K and the slightly positive coefficient at 1600 K. As one would expect, increasing the rate of this reaction shortens the ignition delay time as it produces ethylene and propanoic acid faster and it is the ethylene chemistry and, in particular, the vinyl chemistry that largely controls ignition at low temperatures. At high temperature, increasing this reaction starts to inhibit the production of the fuel-radical species, which are important under these conditions due to the decreased reactivity of vinyl plus O_2.

Figures 15 and 16 show the effect of the decomposition of the most important fuel-radical species, EP2J, it being the predominant fuel-radical produced because it is the site of the

weakest C−H bond. It primarily decomposes through a channel producing methyl ketene and $C_2H_5\dot{O}$, Figure 12. Increasing this rate decreases the reactivity as less of it progresses through the other, more reactive channels, namely the one producing EPMJ. EPMJ produces ethylene, which increases reactivity, particularly at low temperature. The channel producing EP1D and a $\dot{H}$ atom does not occur under normal conditions but has a small negative sensitivity coefficient when its rate is doubled as it begins to compete with the other two channels. The reactions of EP2J become more important under fuel-lean conditions, as it is present in a greater concentration due to the increased importance of hydrogen abstraction reactions from the fuel.

The results shown in Figure 16 are under conditions identical to those depicted in Figure 15, but these have lower sensitivity coefficients in the range ±10%. Once again it is evident how the sensitivity of the reactions changes with temperature. Increasing the rate of the reaction

$$C_2H_5COOH + \dot{O}H \rightarrow CH_3\dot{C}HCOOH + H_2O$$

produces a positive coefficient at 1200 K and a negative coefficient at 1600 K. At 1200 K, this reaction competes for hydroxyl radicals with the promoting reaction of ethylene plus hydroxyl radical discussed above, thus explaining the positive sensitivity. At higher temperatures, as the importance of ethylene chemistry declines due to vinyl plus O_2 predominantly undergoing a propagation step, it actually increases reactivity by producing hydroxyl radicals and $\dot{H}$ atoms through secondary reactions.

$$CH_3\dot{C}HCOOH \rightarrow CH_3CHCO + \dot{O}H$$

$$CH_3\dot{C}HCOOH \rightarrow C_2H_3COOH + \dot{H}$$

The reaction between propanoic acid and atomic hydrogen

$$C_2H_5COOH + \dot{H} \rightarrow \dot{C}H_2CH_2COOH + H_2$$

shows a significant change in sensitivity as the temperature and equivalence ratio (Figure 16) are changed. It has a positive sensitivity coefficient simply because increasing it consumes H atoms that otherwise would react with molecular oxygen. As the importance of $\dot{H} + O_2 \rightarrow \dot{O} + \dot{O}H$ increases with increasing temperature and with increasing oxygen concentration, propanoic acid also has a greater negative influence on the reactivity.

The other noteworthy reaction shown in Figure 16 is the decomposition of propanoic acid to a methyl radical and a radical of acetic acid:

$$C_2H_5COOH \rightarrow \dot{C}H_3 + \dot{C}H_2COOH$$

This reaction only becomes important at higher temperatures due to its relatively high activation energy.

Figures 15 and 16 show how the sensitivity of the hydrogen abstraction reactions producing the fuel-radical species depicted in Figure 11 is significantly increased under fuel-lean conditions. This is due to the increased concentration of radical species (mainly $\dot{O}$ and $\dot{O}H$) with the ability to abstract a $\dot{H}$ atom from the fuel. Figure 15 shows the large increase in the positive sensitivity coefficient for the production of EP2J, which is the fuel-radical species produced in the largest amount. Increasing the formation of this radical decreases the reactivity by approximately 15% at $\phi = 0.25$ and 1200 K. This decrease in reactivity is brought about because this leads to a *decrease* in the production of ethylene through the six-centered unimolecular decomposition channel from the fuel. Oxidation of ethylene leads to the formation of vinyl radicals, which controls the reactivity of the system, particularly at lower temperatures. Increasing the production of the other three fuel-radical species produces a similar effect but to a lesser extent as they are produced in smaller amounts relative to the EP2J radical.

5. Conclusions

A shock tube study has been carried out for ethyl propanoate and methyl butanoate, model components of biodiesel, over a range of equivalence ratios at pressures of 1 and 4 atm in which ignition delay times were recorded behind the reflected shock wave. Detailed chemical kinetic mechanisms have been developed and used to simulate these data, with the simulated ignition delay times in good agreement with the experimental data; the effects of changes in reflected-shock temperature and pressure, and the effect of varying fuel and oxygen concentrations are all well reproduced.

Due to the importance of ethylene and propanoic acid to the combustion of ethyl propanoate, the developed model was tested against shock tube data for both ethylene and propanoic acid, and also against a range of jet-stirred reactor data for ethylene. Overall, simulations were in good agreement with the experimental data examined.

The reactivity of ethyl propanoate under shock tube conditions of $\phi = 1.0$ at 1 and 4 atm was compared to that of methyl butanoate. It was found that under these conditions, ethyl propanoate ignited faster than methyl butanoate. This was not due to the low activation energy elimination reaction, but due to the reactivity of the products formed, namely ethylene and propanoic acid.

A sensitivity analysis was carried out for ethyl propanoate in an attempt to gain an understanding of the important reactions controlling its oxidation. The results highlighted the importance of ethylene/vinyl chemistry to the overall reactivity of ethyl propanoate.

Acknowledgment. W.M. thanks the Environmental Protection Agency of Ireland for a Doctoral Fellowship (2004-PHD4-8-M1). S.D. thanks the Research Frontiers Programme of Science Foundation Ireland for financial assistance (2004/BR/C0146).

References and Notes

(1) Graboski, M. S.; McCormick, R. L. *Prog. Energy Combust. Sci.* **1998**, *24*, 125−164.
(2) Miyamoto, N.; Ogawa, H.; Nurun, N. M.; Obata, K.; Arima, T. *SAE Pub.* **1998**, SAE-980506.
(3) Simmie, J. M. *Prog. Energy Combust. Sci.* **2003**, *29*, 599−634.
(4) Knothe, G.; Bagby, M. O.; Ryan, T. W., III. *J. American Oil Chem. Soc.* **1998**, *75* (8), 1007−1013.
(5) Parsons, B. I.; Danby, C. J. *J. Chem. Soc.* **1956**, 1795−1798.
(6) Parsons, B. I.; Hinshelwood, C. *J. Chem. Soc.* **1956**, 1799−1803.
(7) Parsons, B. I. *J. Chem. Soc.* **1956**, 1804−1809.
(8) Hoare, D. E.; Li, T.-M.; Walsh, A. D. *Proc. Combust. Inst.* **1967**, *11*, 879−887.
(9) Archambault, D.; Billaud, F. *J. Chim. Phys.* **1999**, *96*, 778−796.
(10) Fisher, E. M.; Pitz, W. J.; Curran, H. J.; Westbrook, C. K. *Proc. Combust. Inst.* **2000**, *28*, 1579−1586.
(11) Marchese, A. J.; Angioletti, M.; Dryer, F. L. 30th Symposium (International) on Combustion, Chicago, July 25−30, 2004; Work-in-progress poster 1F1-03.
(12) Gaïl, S.; Thomson, M. J.; Sarathy, S. M.; Syed, S. A.; Dagaut, P.; Diévart, P.; Marchese, A. J.; Dryer, F. L. *Proc. Combust. Inst.* **2007**, *31*, 305−311.
(13) Schwartz, W. R.; McEnally, C. S.; Pfefferle, L. D. *J. Phys. Chem.* **2006**, *110*, 6643−6648.
(14) Ben-Dor, G.; Igra, O.; Elperin, T.; Lifshitz, In. A. *Handbook of Shock Waves*; Academic Press: New York, 2001; Vol. 3, pp 212−256.
(15) Morley, C. http://www.gaseq.co.uk/.

(16) Smith, J. M. Ph.D. Thesis, National University of Ireland, Galway, 2004.
(17) Michael, J. V.; Sutherland, J. W. *Int. J. Chem. Kinet.* **1986**, *18*, 409−436.
(18) Horning, D. C.; Davidson, D. F.; Hanson, R. K. *Int. Symp. Shock Waves, 23rd* **2001**, paper 5732.
(19) Lund, C. M.; Chase, L. "HCT - A General Computer Program for Calculating Time-Dependent Phenomena Involving One-Dimensional Hydrodynamics, Transport, and Detailed Chemical Kinetics," Lawrence Livermore National Laboratory report UCRL-52504, revised (1995).
(20) Benson, S. W. *Thermochemical Kinetics*; John Wiley and Sons, Inc.: New York, 1976.
(21) Ritter, E. R.; Bozzelli, J. W. *Int. J. Chem. Kinet.* **1991**, *23*, 767−778.
(22) Lay, T.; Bozzelli, J. W.; Dean, A. M.; Ritter, E. R. *J. Phys. Chem.* **1995**, *99* (39), 14514−14527.
(23) Sumathi, R.; Green, W. H., Jr. *Phys. Chem. Chem. Phys.* **2003**, *5*, 3402−3417.
(24) Mallard, W. G.; Westley, F.; Herron, J. T.; Hanson, R. F. *NIST Standard Reference Database 17 2Q98*; NIST: Gaithersburg, MD, 1994.
(25) *NIST Chemistry WebBook*; Linstrom, P. J., Mallard, W. G., Eds.; NIST Standard Reference Database Number 69; National Institute of Standards and Technology: Gaithersburg, MD, 20899, March 2003 (http://webbook.nist.gov).
(26) Ó Conaire, M.; Curran, H. J.; Simmie, J. M.; Pitz, W. J.; Westbrook, C. K. *Int. J. Chem. Kinet.* **2004**, *36*, 603−622.
(27) El-Nahas, A. M.; Bozzelli, J. W.; Simmie, J. M.; Curran, H. J.; Metcalfe, W.; Dooley, S. *J. Phys. Chem. A*, in press.
(28) Curran, H. J. *Int. J. Chem. Kinet.* **2006**, *38*, 250−275.
(29) Bozzelli, J. W.; Dean, A. M. *J. Phys. Chem.* **1990**, *94*, 3313−3317.
(30) Troe, J. *Phys. Chem. Chem. Phys.* **1974**, *78* (5), 478−488.
(31) O'Neal, H. E.; Benson, S. W. *J. Phys. Chem.* **1967**, *71*, 2903−2921.
(32) Blades, A. T.; Sandhu, H. S. *Int. J. Chem. Kinet.* **1971**, *3*, 187−193.
(33) Kaiser, E. W.; Wallington, T. J.; Hurley, M. D.; Platz, J.; Curran, H. J.; Pitz, W. J.; Westbrook, C. K. *J. Phys. Chem. A* **2000**, *104* (35), 8194−8206.
(34) Fischer, S. L.; Dryer, F. L.; Curran, H. J. *Int. J. Chem. Kinet.* **2000**, *32*, 713−740.
(35) Curran, H. J.; Fischer, S. L.; Dryer, F. L. *Int. J. Chem. Kinet.* **2000**, *32*, 741−759.
(36) Zheng, X. L.; Lu, T. F.; Law, C. K.; Westbrook, C. K.; Curran, H. J. *Proc. Combust. Inst.* **2005**, *30*, 1101−1109.
(37) Marinov, N. M. *Int. J. Chem. Kinet.* **1999**, *31*, 183−220.
(38) Curran, H. J.; Gaffuri, P.; Pitz, W. J.; Westbrook, C. K. *Combust. Flame* **1998**, *114*, 149−177.
(39) Curran, H. J.; Gaffuri, P.; Pitz, W. J.; Westbrook, C. K. *Combust. Flame* **2002**, *129*, 253−280.
(40) Doolan, K. R.; Mackie, J. C.; Reid, C. R. *Int. J. Chem. Kinet.* **1986**, *18*, 575−596.
(41) Hatakeyama, S.; Honda, S.; Washida, N.; Akimoto, H. *Bull. Chem. Soc. Jpn.* **1985**, *58*, 2157.
(42) Horning, D. C.; Davidson, D. F.; Hanson, R. K. *J. Propul. Power* **2002**, *18*, 363−371.
(43) Westbrook, C. K.; Thornton, M. M.; Pitz, W. J.; Malte, P. C. *Proc. Combust. Inst.* **1988**, *22*, 863−871.
(44) Dagaut, P.; Boettner, J.-C.; Cathonnet, M. *Int. J. Chem. Kinet.* **1990**, *22*, 641−664.
(45) Brown, C. J.; Thomas, G. O. *Combust. Flame* **1999**, *117*, 861−870.